J. Fluid Mech. (1987), *vol.* 178, *pp.* 441–457
Printed in Great Britain

Waves on a static water surface beneath a layer of moving air

By I. H. GRUNDY AND E. O. TUCK
Applied Mathematics Department, University of Adelaide, GPO Box 498, Adelaide, South Australia 5001, Australia

(Received 13 December 1985 and in revised form 29 July 1986)

Large-amplitude waves can exist on an air–water interface where the air is in steady non-uniform flow and the water is stationary. Computations of such waves are provided here, both for periodic nonlinear Stokes-like waves, and for a specific wave-making configuration in which the periodic solution appears as the downstream far field. The wavemaker geometry chosen here is relevant to the edge region of a hovercraft, and the large-amplitude free-surface disturbance caused by the escaping air is computed as a function of the Froude number based on air-jet velocity and thickness.

1. Introduction

If air is caused to move in a non-uniform manner above a water surface, that surface will deform under the action of the non-uniform aerodynamic pressure, whether or not the water moves. We consider here only those cases where the water remains at rest, or in which its motion can be neglected relative to that of the air. In such cases, the equilibrium free-surface configuration represents a balance between aerodynamic and hydrostatic pressures.

The boundary condition on the interface between air and water can be shown (Tuck 1975) to be equivalent to that for moving water with a constant-pressure free surface. Some well-known water-wave solutions (e.g. deep-water Stokes waves, as computed by Schwartz 1974) can simply be turned upside down and re-interpreted as relevant to the present context. However, an interesting class of problems that does not have a direct water-wave analogue is that in which the air layer is of finite thickness, its upper boundary being a constant-speed free streamline.

An example of such a flow is a vertically downward jet of air impinging upon the water surface, where it splits symmetrically and then spreads out over the surface, generating waves in the process. This problem was studied first by Olmstead & Raynor (1964), and more recently by Vanden-Broeck (1981). It is the purpose of the present paper to study another (unsymmetric) example of a generating mechanism, as well as to investigate in their own right the nonlinear waves that are generated.

As an idealized model of the edge-seal zone of a hovercraft (see e.g. Trillo 1971; Tsel'nik 1982), or the trailing edge of an airfoil flying close above water (Tuck 1985; Grundy 1986), consider the steady irrotational flow sketched in figure 1. Air (assumed inviscid and incompressible) is caused to flow inward from infinity on the left, in a sink-like maner, in a sector region bounded by a plane wall and a static water surface. The air then passes through a gap beneath the lower edge of the wall and the water, and emerges on the right as a jet, that flows to infinity in a layer above the water surface. Neglect of air viscosity means that we are neglecting the developing

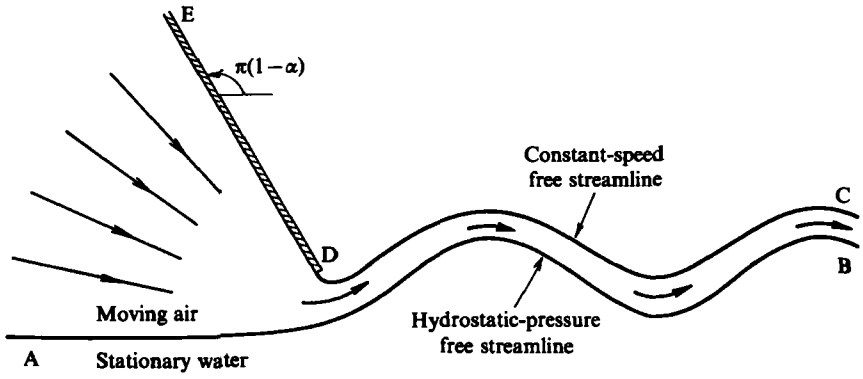

FIGURE 1. Sketch of flow in the physical (x, y)-plane.

boundary layers at the air–air and air–water interfaces, an assumption that can be expected to provide a reasonable approximation for rapid air flow not too far from the gap, before the layer breaks up.

So long as the air layer does retain its identity, as it moves to the right, it generates an asymptotically periodic wave on the gravity-dominated air–water interface, and one of our tasks is to compute the amplitude of this wave, as a function of forcing parameters such as the net volume flux of air and the gap width. The wave is small only when the air flux is small, or, more precisely, when a suitable Froude number based on this flux is small. In the limit when this Froude number tends to zero, the water surface appears as a rigid wall, and the air jet flows over that wall in a non-wave-like manner. This is a standard free-streamline problem, and the solution can be obtained easily in closed form by hodograph methods.

Our generalization to finite Froude number allows the water surface to deform, and we reduce this problem to a nonlinear integral equation for the hodograph variables (velocity magnitude and direction) along the air–water free boundary. This integral equation is then solved numerically for various values of the Froude number and wall angle.

As the Froude number increases from zero (in effect, as we blow harder relative to the available gap), the violence of the disturbance to the water surface increases, and the amplitude of the far-field waves increases. However, we find that, at least in theory, extremely steep waves can be generated, with amplitudes many times the gap width or the air-layer thickness. In practice, such large free-surface deformations would suggest a break up in the form of spray, or detachment of the air jet from the water surface, as discussed by Tsel'nik (1982).

In order to throw more light on these large-amplitude waves, we also provide here an independent study of the far-field limit, i.e. of purely periodic plane waves on an interface between dynamic air and static water. For this purpose, a simple Fourier series representation of the solution is truncated to a finite number of terms, the coefficients of which are then found by collocation of the boundary condition.

In the limit where the air-layer thickness is far in excess of the wavelength, these waves are exactly the same as deep-water plane progressive (Stokes) waves, turned upside down. Such a 'deep-layer' wave has the usual maximum steepness (trough-to-crest height/wavelength) of about 0.141, and is limited by development of a stagnation point in a 120° angle, but at the trough rather than the crest. However, finite air-layer thickness has the opposite effect to that of finite water depth on Stokes

waves, in that it allows the steepness to increase above 0.141. For large-to-moderate layer thicknesses, the limiting wave of maximum steepness still has a stagnation point at the trough. However, for moderate-to-small layer thicknesses, the waves become so steep (amplitudes comparable to wavelength) that they are no longer so limited, but continue to steepen until the upper air surface self-intersects. Meanwhile, the air-layer thickness is becoming small relative to the wavelength, and a 'shallow-layer' theory equivalent to that used by Peregrine (1974) can be applied.

2. Problem formulation

We consider steady irrotational flow of (incompressible) air in a region whose only boundaries consist of a semi-infinite plane wall at an angle $\pi(1-\alpha)$ to the horizontal, and a static water surface, as depicted in figure 1. To an observer in the upstream far field, the flow appears to be that generated by a sink, located in the gap between the bottom edge of the wall and the water. That is, the flow upstream is directed radially inward, and has a prescribed net volume flux ψ_0. Consequently, stagnation conditions apply at upstream infinity, and the water surface approaches its minimum height there.

At the bottom edge of the wall, the air flow is assumed to detach smoothly, forming a jet lying above and in contact with the water, and subsequently extending to downstream infinity. The effect of gravity is neglected in this air jet, the pressure then being given by

$$p = p_0 - \tfrac{1}{2}\rho_A q^2, \tag{2.1}$$

where p_0 is the stagnation pressure, ρ_A is the density of air, and q is the magnitude of the air velocity.

The upper surface of the jet is a free streamline, on which the pressure has the constant (atmospheric) value p_A. Thus, on this surface, q is constant and equal to U, where

$$U = \left(\frac{p_0 - p_A}{\tfrac{1}{2}\rho_A}\right)^{\frac{1}{2}} \tag{2.2}$$

is known if the two pressures p_0, p_A are known. In the hovercraft application, $p_0 - p_A$ is the excess pressure induced by the hovercraft's fans, and one output of interest is the manner in which p_0 decays to p_A along the air stream.

On the lower surface of the jet, the pressure in the air must equal that in the water, and the latter is hydrostatic, since we are assuming that the water does not move. Thus, on this air–water interface, we have

$$p = p_0 - \rho_W g(y - y_S), \tag{2.3}$$

where ρ_W is the density of water, g is the acceleration due to gravity, and $y - y_S$ is the free-surface elevation relative to the upstream stagnation level $y = y_S$. The bottom edge of the wall is taken as the origin $y =$. Equating (2.1) and (2.3) gives

$$\tfrac{1}{2}q^2 - g\frac{\rho_W}{\rho_A}(y - y_S) = 0 \tag{2.4}$$

as the free-surface condition on the (dynamic air)–(static water) interface. This is (cf. Tuck 1975) the same as for a constant-pressure surface of dynamic water turned upside down, with a negative effective gravity scaled by the density ratio.

A quantity of particular interest is the 'mean' downstream water level $y = y_A$,

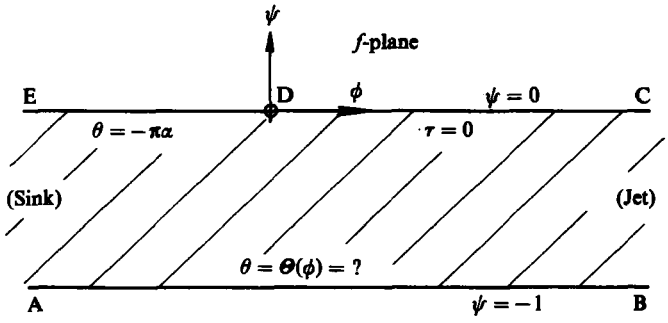

FIGURE 2. Flow domain in f-plane.

which would occur in a hypothetical undisturbed stream of air at speed U and pressure p_A. Thus

$$y_A = y_S + \frac{1}{2}\frac{\rho_A}{\rho_W g} U^2. \tag{2.5}$$

If the air flow did not induce any waves, the decrease in pressure from p_0 to p_A would simply cause the water surface to rise monotonically from $y = y_S$ to $y = y_A$. However, as we shall see, this does not happen, and the situation far downstream consists instead of a stream of air of speed close to U flowing over a water surface that is deformed into an asymptotically periodic wave whose mean level is close to $y = y_A$. It should be noted that y_A could be either positive or negative, and that if it is positive, the bottom edge of the wall dips beneath the mean water level.

The coordinate system is now non-dimensionalized so that the incoming net volume flux ψ_0 and the flow velocity U on the upper air boundary are both scaled to unity. Our characteristic lengthscale is thus $d = \psi_0/U$, where d can be interpreted as the mean air-layer thickness. Equation (2.4) can now be rewritten in non-dimensional form as

$$y = y_S + \tfrac{1}{2}F^2 q^2, \tag{2.6}$$

where here and subsequently, all coordinates such as y are scaled with respect to d, and all velocities such as q with respect to U. The Froude number F is defined as

$$F = \left(\frac{\rho_A}{\rho_W}\right)^{\frac{1}{2}} \frac{U}{(gd)^{\frac{1}{2}}}, \tag{2.7}$$

and we shall also write $\gamma = F^{-2}$.

We shall use the complex coordinate $z = x + iy$ and velocity potential $f = \phi + i\psi$, seeking an analytic function $z = z(f)$. The streamline $\psi = 0$ consists of the wall and the upper free surface of air, while the streamline $\psi = -1$ consists of the air–water interface. The origin in both z- and f-planes is taken at the bottom edge of the wall. The flow region in the f-plane is a strip, as shown in figure 2.

We now introduce the logarithmic hodograph variable

$$\Omega = \tau - i\theta = -\log\frac{dz}{df}, \tag{2.8}$$

where $\tau = \log q$ is zero on the upper free boundary $\psi = 0$, $\phi > 0$, while θ is the angle between streamlines and the z-axis, and takes the constant value $-\pi\alpha$ on the wall $\psi = 0$, $\phi < 0$. On the air–water interface $\psi = -1$, neither τ nor θ is given, but there

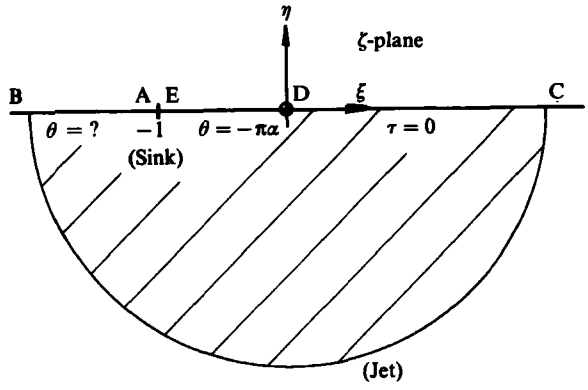

FIGURE 3. Flow domain in the ζ-plane.

is a relation between them, as follows. Upon differentiating (2.3), substituting $q = e^{\tau}$, and using (2.6), we find

$$e^{3\tau}\frac{\partial \tau}{\partial \phi} = \gamma \sin\theta, \tag{2.9}$$

or, on integrating

$$e^{3\tau} = 3\gamma \int_{-\infty}^{\phi} \sin\theta \, d\varphi, \tag{2.10}$$

The strip in the f-plane is mapped to the lower half-ζ-plane (see figure 3) using the transformation

$$\zeta = e^{\pi f} - 1 \tag{2.11}$$

and ζ will be used temporarily as an independent variable in place of f. The line segment CD in the f-plane representing the upper free boundary is mapped to the positive real axis. The upstream stagnation zone EA at infinity is mapped to the point $(-1, 0)$. The segments DE and AB, representing the wall and the air–water interface respectively are mapped to the negative real axis, onto the intervals $(-1, 0)$ and $(-\infty, -1)$ respectively.

At upstream infinity, we can write the leading-order sink-like flow behaviour as

$$z \to e^{i\pi(1-\alpha)}[k\, e^{-\pi\alpha f} + c], \quad \phi \to -\infty, \tag{2.12}$$

where k and c are real constants which depend on the local flow details in the gap. Thus, as $\phi \to -\infty$,

$$\Omega \to \pi\alpha f - \log \pi\alpha k + i\pi\alpha. \tag{2.13}$$

It follows then from (2.11) and (2.13) that Ω is logarithmically singular at $\zeta = -1$. At downstream infinity, that is, as $\phi \to +\infty$, or $|\zeta| \to +\infty$, Ω is bounded. The real part of Ω is thus known on the positive real ζ-axis, and the form of the imaginary part is specified on the negative real ζ-axis (even if the exact details are not yet known on the air–water interface). This suggests that we should define a new variable

$$\chi(\zeta) = \zeta^{-\frac{1}{2}}\Omega, \tag{2.14}$$

with the useful properties that the real part of χ is specified, in the above sense, everywhere on the real axis, and that $\chi \to 0$ as $|\zeta| \to +\infty$. Also, since Ω is bounded at $\zeta = 0$, $\chi(\zeta)$ remains integrable there, and $\chi(\zeta)$ can also be seen to be integrable at $\zeta = -1$.

Application of Cauchy's theorem to χ in the lower half-plane then gives

$$-\pi i\chi(\zeta) = \int_{-\infty}^{+\infty} \frac{\chi(\xi)\,d\xi}{\xi-\zeta} \tag{2.15}$$

for all ζ on the real axis. Expressions for π and θ on the negative real and positive real ζ-axes respectively can now be extracted by rewriting the left-hand side of (2.15) in terms of Ω and taking the real part of both sides. Thus

$$\tau(\zeta) = \frac{1}{\pi}|\zeta|^{\frac{1}{2}} \int_{-\infty}^{-1} \frac{\theta(\xi)\,d\xi}{|\xi|^{\frac{1}{2}}(\xi-\zeta)} + \alpha \log\left|\frac{|\zeta|^{\frac{1}{2}}-1}{|\zeta|^{\frac{1}{2}}+1}\right|, \quad \zeta < 0 \tag{2.16}$$

and

$$\theta(\zeta) = -\frac{1}{\pi}|\zeta|^{\frac{1}{2}} \int_{-\infty}^{-1} \frac{\theta(\xi)\,d\xi}{|\xi|^{\frac{1}{2}}(\xi-\zeta)} - 2\alpha \arctan|\zeta|^{-\frac{1}{2}}, \quad \zeta > 0. \tag{2.17}$$

The logarithmic and arctan terms derive from the interval $(-1, 0)$, on which $\theta(\zeta)$ is known and constant, and over which the integral in (2.15) can be evaluated analytically. In fact, if $\theta(\zeta) \equiv 0$ for $\zeta < -1$, these terms provide the exact solution (cf. Gilbarg 1960) when the air–water surface is replaced by a rigid wall. Note that the integral in (12.15) is of the Cauchy-principal-value type, and hence so is (2.16) if $\zeta \in (-\infty, -1)$; that is, for points along the air–water interface.

Equation (2.16) can be rewritten in the original ϕ-variables on $\psi = -1$, letting $\tau = T(\phi)$ and $\theta = \Theta(\phi)$ on this streamline, to obtain

$$T(\phi) = (1+e^{\pi\phi})^{\frac{1}{2}} \int_{-\infty}^{+\infty} \frac{\Theta(\varphi)\,e^{\pi\varphi}\,d\varphi}{(1+e^{\pi\varphi})^{\frac{1}{2}}(e^{\pi\phi}-e^{\pi\varphi})} + \alpha\pi\phi - 2\alpha\pi \log|1+(1+e^{\pi\phi})^{\frac{1}{2}}|. \tag{2.18}$$

It is clear that we can now combine (2.18) with (2.10), also rewritten in terms of ϕ, by the elimination of $T(\phi)$, to give a single nonlinear integral equation for our fundamental unknown $\Theta(\phi)$, namely

$$3\gamma \int_{-\infty}^{\phi} \sin\Theta(\varphi)\,d\varphi - e^{3\alpha\pi\phi}\,|1+(1+e^{\pi\phi})^{\frac{1}{2}}|^{-6\alpha\pi} \times \exp\left[3(1+e^{\pi\phi})^{\frac{1}{2}} \int_{-\infty}^{+\infty} \frac{\Theta(\varphi)\,e^{\pi\varphi}\,d\varphi}{(1+e^{\pi\varphi})^{\frac{1}{2}}(e^{\pi\phi}-e^{\pi\varphi})}\right] = 0. \tag{2.19}$$

In §4 we derive a numerical scheme to determine the solution $\Theta(\phi)$ of the integral equation (2.19) for given γ (i.e. given F) and α.

Once $\Theta(\phi)$ is known, τ and θ can be determined around the flow boundaries by substitution into (2.16) and (2.17). The physical coordinates $z(f)$ then follow by integration of (2.8).

3. Numerical Method

The numerical scheme we shall follow is similar to that devised by Vanden-Broeck (1981), with the exception that we have used the integrated form of the aerodynamic–hydrostatic free-surface condition (2.10) to eliminate $T(\phi)$ completely.

We begin by replacing the infinite range of integration in (2.19) by a finite range $[A, B]$, where A is large and negative, and B is large and positive. Truncation corrections were implemented when necessary to account for the contributions from

$\phi < A$ and $\phi > B$. We now partition the resulting interval $[A, B]$ into N subintervals of equal width. The subinterval end points are thus

$$\phi_j = \left(\frac{B-A}{N}\right) j + A, \quad j = 0, 1, 2, \ldots, N, \tag{3.1}$$

at which

$$\Theta(\phi_j) = \Theta_j, \quad j = 0, 1, 2, \ldots, N. \tag{3.2}$$

We also need the N subinterval midpoints

$$\phi_{i-\frac{1}{2}} = \frac{\phi_{i-1} + \phi_i}{2}, \quad i = 1, 2, \ldots, N. \tag{3.3}$$

We apply the trapezoidal rule to both the integrals in (2.19), using as nodes the $N+1$ points where $\phi = \phi_j$. Our aim is thus to write the integrals in (2.19) as summations involving the Θ_j as sole unknowns. We now seek to satisfy (2.19) at each of the N midpoints $\phi_{i-\frac{1}{2}}$, $i = 1, 2, \ldots, N$. At a particular i, the first integral involves integration only up to the midpoint of the ith subinterval, thus requiring knowledge of $\Theta(\gamma_{i-\frac{1}{2}})$. Four-point Lagrange interpolation is used to rewrite this quantity in terms of Θ_{i-1}, Θ_i, Θ_{i+1} and Θ_{i+2}. The second (Cauchy-principal-value) integral can be evaluated as if it were an ordinary integral, ignoring the singularity, owing to the symmetry of the discretization (cf. Monacella 1967).

We now have a system of N nonlinear algebraic equations involving the $N+1$ unknowns Θ_i, $i = 0, 1, 2, \ldots, N$. We reduce by one the number of unknowns by assuming that $\Theta_0 = 0$. That is, we assume that the interface is flat at the furthest upstream point $\phi = A$, which is valid for sufficiently large $|A|$. A truncation correction, using the fact that $\Theta(\phi)$ decays like a multiple of $e^{3\alpha\pi\phi}$ as $\phi \to -\infty$, was necessary for computation at small α. However, simply setting $\Theta_0 = 0$ was adequate for most values of $|A|$ used. Downstream, use of a truncation correction at $\phi_N = B$, was found to be necessary for large values of F i.e. $F > 3$, and the crude approximation, $\Theta = \Theta_N$ for $\phi > B$, was adequate.

The final system of N equations in N unknowns is solved using Newton's method, and an apparently unique solution is found at each F and α. In most cases, the rigid-ground solution ($\Theta \equiv 0$) is a useful initial guess for the Newton scheme. Whenever this is not true, converged solutions at one value of F can be used as initial guesses for computations at nearby F-values. At fixed F, it is also possible to vary α, using the previous converged solutions at nearby values of α as initial guesses. For any sensible starting guesses, convergence of Newton's method to five- or six-figure accuracy is obtained within 7 iterations.

At fixed grid size, we vary the positions of $\phi_0 = A$ and $\phi_N = B$ until the results in the region of interest are independent of their position. The discretization error can then be decreased further by decreasing the grid size (i.e. by increasing N), at fixed A and B, until the required accuracy is obtained. Close to three-figure accuracy can be attained with a grid size of 0.2 (for example with $A = -5$ and $N = 100$).

In most cases we wish to compute at least one, and preferably two, complete downstream waves. This forces $\phi_N = B$ further downstream than is dictated by truncation-error considerations. At high values of F, for example $F > 3$, where the wavelength in terms of ϕ is also large, large numbers of points must be used to compute even one complete wave.

Once a converged solution for $\Theta(\phi)$ is obtained, the actual shapes of both the air–water interface $\psi = -1$ and the upper free streamline $\psi = 0$ are each easily

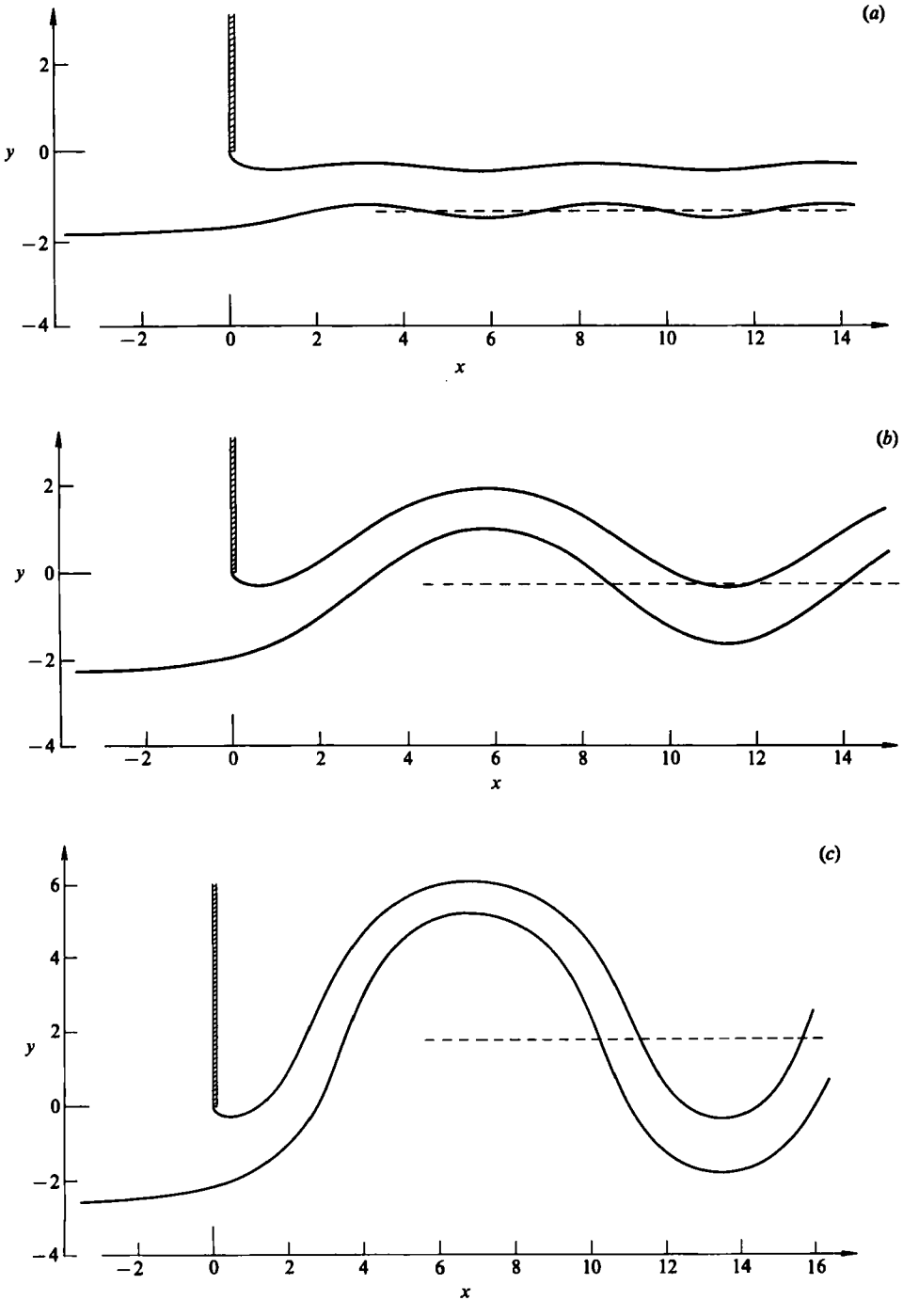

FIGURE 4. Physical-plane profile for the vertical-wall case, $\alpha = 0.5$. The 'mean' downstream water level $y = y_A$ is shown dashed. (*a*) $F = 1$; (*b*) 2; (*c*) 3.

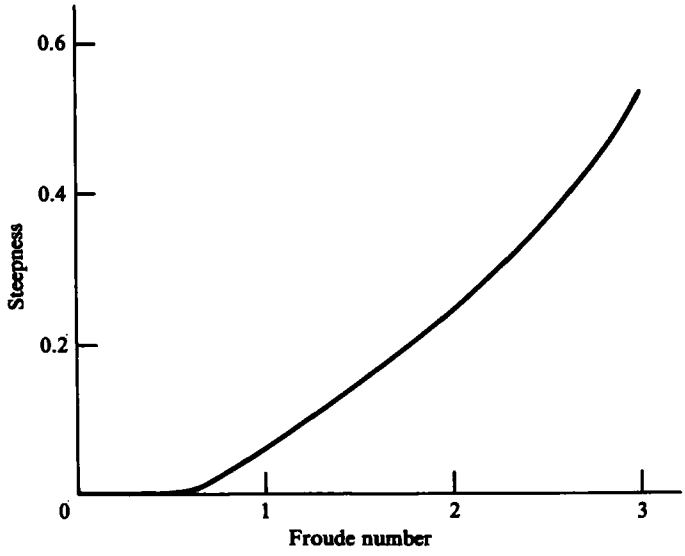

FIGURE 5. Plot of steepness as a function of F for the vertical wall.

computed separately, by numerical integration of (2.8). Their *relative* positions, however, depend on two constants of integration which are directly related to the values of k and c in (2.12). The value of k follows (see (2.13)) from the constant term in the asymptotic expansion as $\phi \to -\infty$ of $T(\phi)$ in (2.18). Once k is found, c is found by integration of (2.8) up the rigid wall, and comparison with (2.12). The x and y constants of integration follow immediately.

4. Computed results

Figure 4 (a–c) shows some physical-plane profiles for various values of F, for the vertical-wall case $\alpha = 0.5$. Typically, near-stagnation conditions are observed within two or three air-layer widths in the sink-like flow upstream of the wall. Downstream, the standing waves supported by the air-layer become periodic very quickly. The first wave differs in size from subsequent waves by less than one percent.

Figures 5, 6, and 7 show the dependence on F of the wave steepness, wavelength, and downstream mean level respectively. In the limit as F tends to zero, both steepness and wavelength tend to zero. That is, for small F (and the results in figure 4 (a) suggest that $F = 1$ is small enough), the waves become asymptotically sinusoidal, and ultimately disappear as F tends to zero. In this (rigid-ground) limit, the mean level y_A shown in figure 7 approaches the constant value $-(\pi+2)/\pi$, i.e. the negative reciprocal of the contraction coefficient for jet flow from a hole. The present computations in fact suggest that the steepness tends to zero *extremely* rapidly with F, so much so that there is an apparent discontinuity in the curve of figure 5 at about $F = 0.6$, the computed steepness being less than 0.001 for $F < 0.5$, say. However, the ability of our program to compute detailed features of such tiny waves is open to question.

As F increases (see figure 4 b, c) the waves become larger, and noticeably nonlinear, developing broad crests and troughs, with steep sides. Accompanying this increase

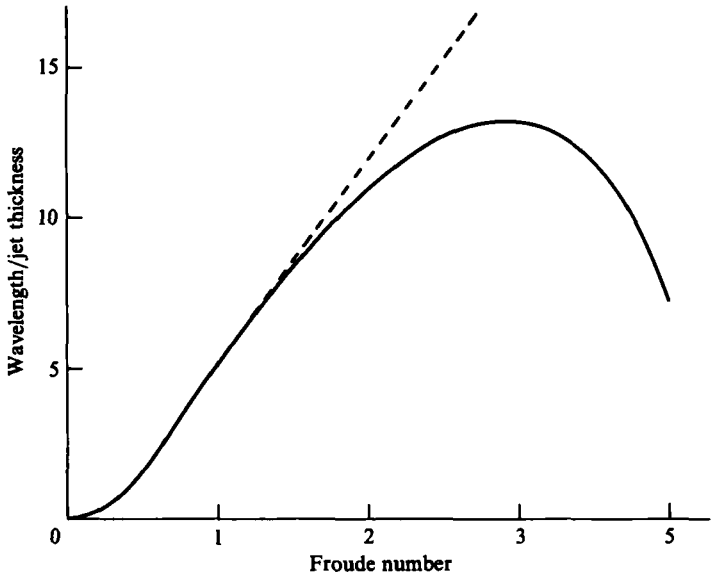

FIGURE 6. Plot of wavelength as a function of F for the vertical wall. The corresponding linearized result (see (5.3)) is shown dashed.

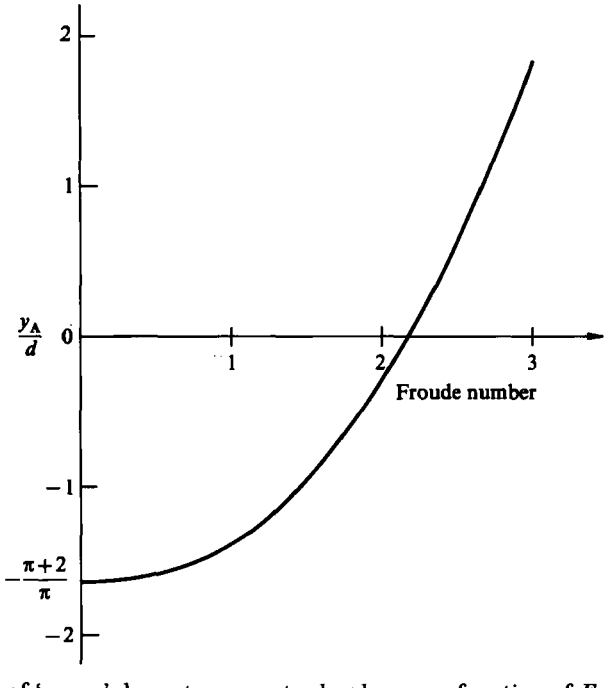

FIGURE 7. Plot of 'mean' downstream water level y_A as a function of F, for the vertical wall.

in wave size is a monotonic increase in y_A. In fact, y_A becomes positive around $F = 2.2$, meaning that for F above this value the wall actually dips below the mean water level. The line $y = y_A$ is shown dashed on each of figure 4(a–c). There is no evidence to suggest that our computations are at all limited to $y_A < 0$.

Beyond $F = 2.2$, figure 5 shows that the steepness of the waves increases without

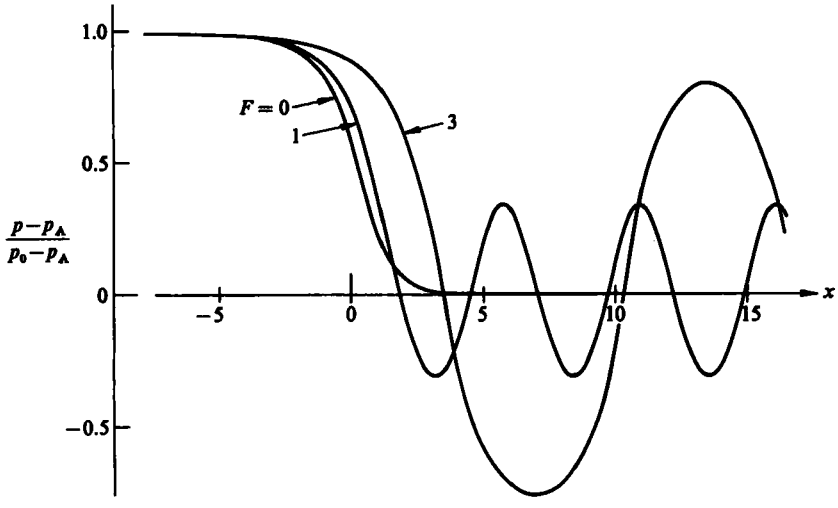

FIGURE 8. Comparison of pressure distributions for the vertical wall at $F = 0$, 1 and 3.

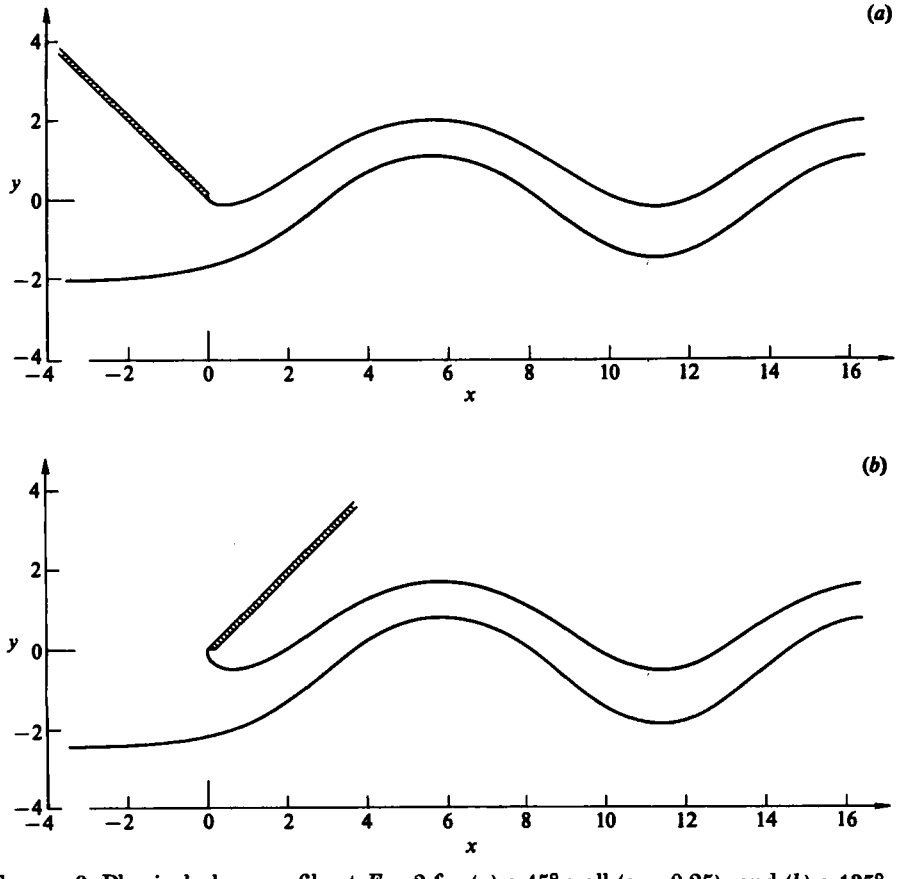

FIGURE 9. Physical-plane profile at $F = 2$ for (*a*) a 45° wall ($\alpha = 0.25$); and (*b*) a 135° wall ($\alpha = 0.75$).

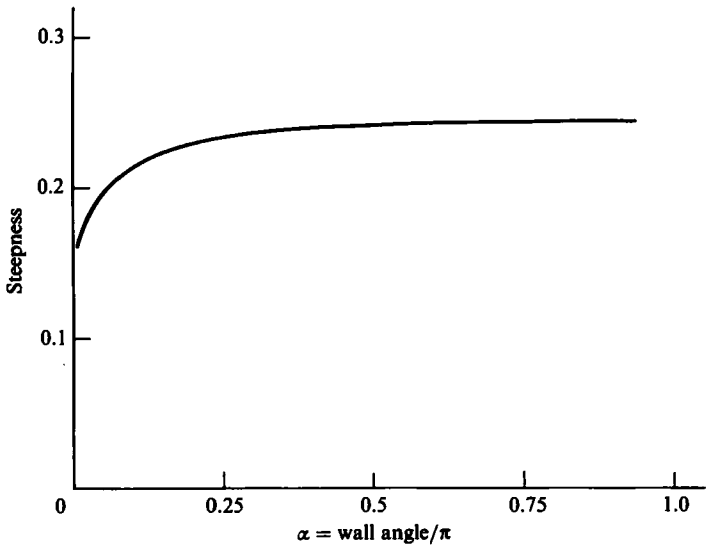

FIGURE 10. Plot of steepness as a function of wall angle parameter α, at $F = 2$.

apparent bound. Figure 6, on the other hand shows that the wavelength reaches a maximum, near $F = 3$. The wave formed appears not to be limited, as Stokes waves are, by the development of a stagnation point at the trough. This behaviour is examined in §5, where the whole family of waves, to which these belong, is discussed in detail.

Figure 8 shows the pressure distribution on the free-surface at various F, including the 'rigid-ground' pressure distribution at $F = 0$. Such results are of some importance for the application to hovercraft and, for example, empirical smoothing of the otherwise step-like variation between p_0 and p_A has been used to compute hovercraft wave resistance (e.g. by Tatinclaux 1976).

So far we have only considered the situation in which F is varied at fixed α, namely $\alpha = 0.5$. We now fix F at a representative value, $F = 2$, and let the wall-angle parameter α vary between 0 and 1. Figures 9(a and b) show physical-plane profiles at $\alpha = 0.25$ and 0.75 respectively. We observe that the position and size of the downstream waves varies very little over this wide range of wall angles. In fact, as α is decreased from unity (see figure 10), there is only a slight decrease in wave steepness until $\alpha = 0.2$. Below this value, however, there is a rapid decrease in steepness and a strong suggestion that this quantity tends to zero as $\alpha \to 0$, i.e. as the flow changes from a sink to a channel-like uniform stream at upstream infinity.

The flow in this limit is of particular interest for application to the trailing edge of an an airfoil in 'ground' effect over water (Tuck 1985; Grundy 1986). In this limit, at any Froude number, there is a possible trivial solution in which the flow continues as a uniform stream, with flat undisturbed free surfaces. As to whether there is also a non-trivial solution, the answer from the present program as $\alpha \to 0$ appears to be no, although conclusive results cannot be obtained for extremely low values of α, i.e. for $\alpha < 0.005$.

For these small values of α, the velocity tends to zero slowly upstream, and it becomes necessary to greatly increase $|A|$, as well as implementing the truncation correction mentioned previously. The number of grid points required becomes

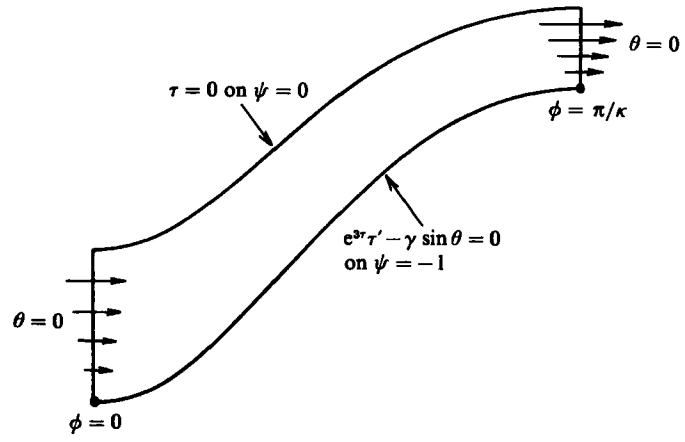

FIGURE 11. Sketch of flow in physical-plane for half of a periodic wave.

prohibitive for $\alpha < 0.005$. In fact, (2.19) fails to hold for uniform stream conditions at upstream infinity, since $T(\phi)$ tends to a constant, and not minus infinity as in the present positive-α problem. Thus, it is no surprise that computation becomes difficult as α tends to zero.

5. The far-field periodic wave

Figure 11 shows a half-wavelength segment of the flow far downstream, which is assumed to have reached an asymptotically periodic state. If κ is the 'wavenumber' in the (ϕ, ψ)-plane, this segment can be assumed to extend from a trough at $\phi = 0$ to a crest at $\phi = \pi/\kappa$. Note that we retain the non-dimensional system used earlier (apart from shifting the origin to a trough) so that κ is scaled by the reciprocal of the net flux ψ_0 of air.

Consider now the series representation (cf. Chen & Saffman 1980)

$$\left.\begin{aligned} \theta &= \sum_{j=1}^{\infty} c_j \sin(j\kappa\phi) \cosh(j\kappa\psi), \\ \tau &= \sum_{j=1}^{\infty} c_j \cos(j\kappa\phi) \sinh(j\kappa\psi). \end{aligned}\right\} \tag{5.1}$$

These series define conjugate harmonic functions that are periodic, period $2\pi/\kappa$, with respect to ϕ. For any choice of the real coefficients c_j, they satisfy $\tau = 0$ on $\psi = 0$, and $\theta = 0$ at both $\phi = 0$ and $\phi = \pi/\kappa$. Only the nonlinear free-surface condition (7) on $\psi = -1$ remains to be satisfied, by appropriate choice of c_j. This condition can be written

$$E(\phi) = e^{3\tau} \frac{\partial \tau}{\partial \phi} - \gamma \sin\theta = 0. \tag{5.2}$$

A simple collocation numerical procedure is then immediately available, in which the series (5.1) are truncated to N terms, and the error $E(\phi)$ defined by (5.2) is forced to vanish at N equally spaced points in $0 < \phi < \pi/\kappa$. This gives N nonlinear algebraic equations in N unknown coefficients c_j, $j = 1, \ldots, N$, which are easily solved by Newton iteration.

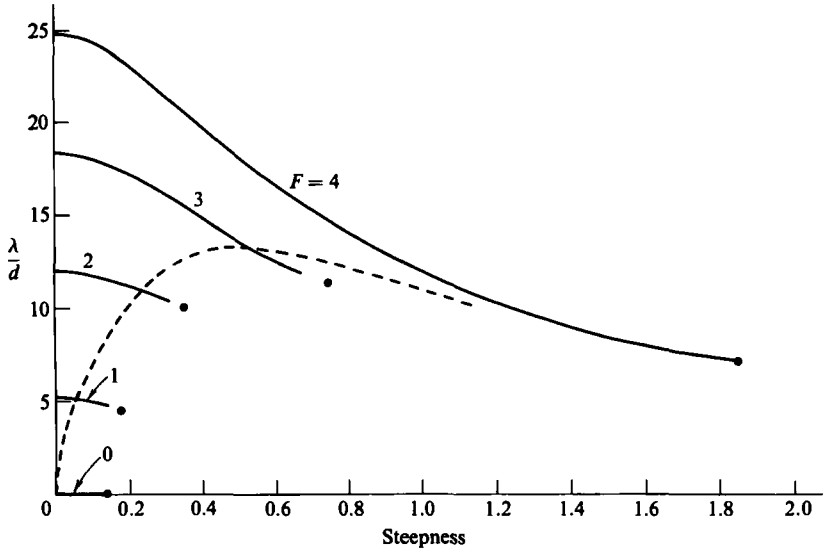

FIGURE 12. Plot of wavelength of periodic waves against steepness, for various values of the Froude number F. Results from the far-field of the hovercraft problem are shown dashed. Dots show estimated highest waves.

The linearized version of the above problem requires only the first term $j = 1$ of the series (5.1), with c_1 (and hence both θ and τ) small. Then (5.2) demands that

$$\gamma = \kappa \tanh \kappa + O(c_1^2), \tag{5.3}$$

a result that was obtained by Vanden-Broeck (1981). The present nonlinear problem is similar to that for classical Stokes waves, as reviewed by Schwartz & Fenton (1982). In fact, the 'deep-water' limit $\kappa \to \infty$ is identical with Stokes waves turned upside-down (cf. Tuck 1975). However, for any finite value of κ, the $\tau = 0$ boundary condition at the upper air boundary is conjugate with that ($\theta = 0$) used on the bottom for finite-depth Stokes waves, and, for example, the equivalent linearized result to (5.3) for such waves would involve 'coth' instead of 'tanh'.

The present program was first checked for very large γ and κ (with γ/κ finite) against deep-water Stokes-wave results of Schwartz (1974). No serious attempt was made to approach the almost-highest type of wave, with steepness 0.141, but a moderately high steepness of 0.12 was achieved with $N = 40$ points at $\gamma/\kappa = 0.868226$, the computed wave speed being 1.07321 times the speed of a linearized wave of the same (true) wavelength, which compares very well with Schwartz's result of 1.07323.

Note that, although the 'wavelength' in the ϕ-variable is $2\pi/\kappa$ in the present formulation, the true physical-plane wavelength is as much an output quantity as is the wave height and profile. These quantities are in fact obtained by direct numerical integration with respect to ϕ, as described earlier. For finite κ, we also integrate with respect to ϕ to obtain the profile of the upper air boundary.

Figure 12 is a compilation of results computed for periodic waves using the method of the present section, together with output from the far field of the hovercraft-type flows treated earlier. This figure provides plots of wavelength versus steepness, parametrized by the Froude number. At any fixed F (or γ)-value, we compute a sequence of flows for increasing steepness, by varying the input parameter κ from

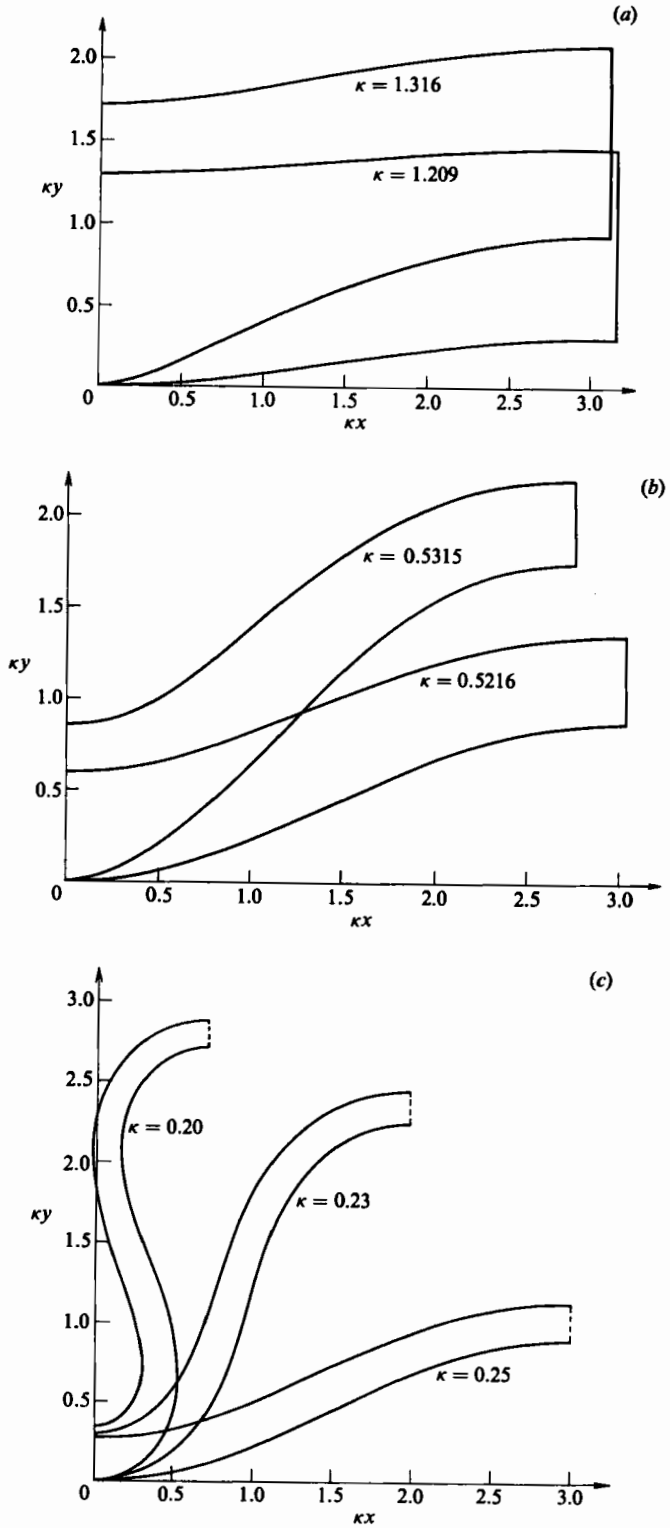

FIGURE 13. Computed profiles of periodic waves at (*a*) $F = 1$; (*b*) 2; (*c*) 4.

the value at zero steepness given by solving (5.3). For F below about 3, as κ increases, the steepness increases, non-linearity becomes more significant, and more terms in the series (5.1) are needed. For F above about 3, κ decreases with steepness. In either case, as the steepness increases, accuracy is eventually lost, and, with $N = 40$, we can only get to within about 90% of the steepest wave using the present simple truncated-series procedure. However, a continuation is shown in figure 12 to a dot near where it is reasonable to believe the steepest wave will occur at each value of F.

Figure 12 also includes (dashed) results from the previous section, for the actual waves produced in the hovercraft-type flow. At each F, the points in the '(steepness–wavelength)'-plane computed in this flow fall very accurately on the appropriate curve computed using the methods of the present section, confirming that the 'far-field waves' have reached a periodic steady state. A curve similar to the dashed curve can be constructed for any wave-making disturbance, e.g. for the vertically downward jet of Olmstead & Raynor (1964).

In classical water-wave theory, the steepest wave is always that with a stagnation point at the crest, where the angle is 120°. The present corresponding 'upside-down' wave would have a stagnation point at the *trough*, and this does indeed appear to be the limiting behaviour, providing F is below about 3. In contrast to the effect of finite depth on classical water waves, which tends to reduce the maximum steepness below the infinite-depth value 0.141 which occurs at $F = 0$, in the present case the maximum steepness is increased by finite-F effects. The air jet thus appears to allow larger waves than could exist on a stream with no such jet.

This phenomenon is displayed even more dramatically at higher Froude numbers, $F > 3$, when it appears that development of a trough stagnation point is no longer a limiting factor, and (at least computationally) there appears to be no limit at all on steepness. However, the results eventually become physically unrealistic, at steepnesses of about 1.8, since the upper air free surface becomes self-intersecting.

Figure 13 (*a–c*) provides examples of computed free-surface shapes. At the lowest Froude number shown ($F = 1$ on figure 13*a*) the air layer is quite thick, and the upper air boundary has a minor effect on the air–water interface. Thus the latter behaves like an upside-down classical wave in water of infinite depth. The two curves shown are for a small steepness, where the wave is quite sinusoidal, and a near-maximum steepness, where the trough is starting to sharpen toward a 120° angle. The actual steepness of this wave (0.150) is already a little greater than the classical value for infinite-depth Stokes waves. Similarly, figure 13(*b*) shows a small and a near-maximum steepness at $F = 2$. Finally, figure 13(*c*) at $F = 4$ shows results at three steepnesses, the greatest of which is just beyond the physically realizable limit, i.e. has a self-intersecting upper free surface.

The waves in figure 13(*c*) have layer thicknesses that are quite small relative to the wavelength, and it is possible to describe their properties in terms of a 'shallow-layer' theory analogous to the shallow-water theory of water waves. Much of the research, such as that of Tsel'nik (1982), on edge-seal effects for hovercraft, makes such shallow-layer or thin-jet assumptions. For periodic waves, a shallow-layer theory has been given in an equivalent context by Peregrine (1974), and the profiles in figure 13(*c*) agree with the cnoidal waves obtained by Peregrine.

REFERENCES

CHEN, B. & SAFFMAN, P. G. 1980 Steady gravity–capillary waves on deep water, II. Numerical results for finite amplitude. *Stud. Appl. Math.* **62**, 95–111.

GILBARG, D. 1960 Jets and Cavities. In *Handbuch der Physik* (ed. S. Flugge), vol. 9, pp. 311–445. Springer.

GRUNDY, I. H. 1986 Airfoils moving in air close to a dynamic water surface. *J. Austral. Math. Soc.* B**27**, 328–347.

MONACELLA, V. J. 1967 On ignoring the singularity in the numerical evaluation of Cauchy principal value integrals. *David Taylor Model Basin Rep. No.* 2356.

OLMSTEAD, W. E. & RAYNOR, S. 1964 Depression of an infinite liquid surface by an incompressible gas jet. *J. Fluid Mech.* **19**, 561–576.

PEREGRINE, D. H. 1974 Surface shear waves. *J. Hydraul. Div.* ASCE **100**, 1215–1227.

SCHWARTZ, L. W. 1974 Computer extension and analytic continuation of Stokes's expansion for gravity waves. *J. Fluid Mech.* **62**, 553–578.

SCHWARTZ, L. W. & FENTON, J. D. 1982 Strongly nonlinear waves. *Ann. Rev. Fluid Mech.* **14**, 39–60.

TATINCLAUX, J. C. 1976 Effect of pressure drop at the bow and stern of an otherwise uniform pressure distribution on the induced wave resistance. *Intl Seminar on Wave Resistance*, pp. 389–390. The Society of Naval Architects of Japan, Tokyo.

TRILLO, R. L. 1971 *Marine Hovercraft Technology.* London: Leonard Hill.

TSEL'NIK, D. S. 1982 On the jet curtain over water. *J. Ship. Res.* **26**, 77–88.

TUCK, E. O. 1975 On air flow over free surfaces of stationary water. *J. Austral. Math. Soc.* B**19**, 66–80.

TUCK, E. O. 1985 A simple one dimensional theory for air-supported vehicles over water. *J. Ship. Res.* **28**, 290–292.

VANDEN-BROECK, J.-M. 1981 Deformation of a liquid surface by an impinging gas jet. *SIAM J. Appl. Math.* **41**, 306–309.